processes

MDPI

Article

An Investigation on Gel-State Electrolytes for Solar Cells Sensitized with β-Substituted Porphyrinic Dyes

Nicola Sangiorgi [1,*], Alex Sangiorgi [1], Alessandra Sanson [1], Maurizio Licchelli [2] and Alessio Orbelli Biroli [2,*]

[1] Institute of Science, Technology and Sustainability for Ceramics-National Research Council of Italy (ISSMC-CNR, Former ISTEC-CNR), Via Granarolo 64, 48018 Faenza, Italy
[2] Dipartimento di Chimica, Università di Pavia, Via Taramelli 12, 27100 Pavia, Italy
* Correspondence: nicola.sangiorgi@istec.cnr.it (N.S.); alessio.orbellibiroli@unipv.it (A.O.B.)

Abstract: The presence of a liquid electrolyte in dye-sensitized solar cells (DSSCs) is known to limit the time stability of these devices due to leakage and evaporation phenomena. To overcome this issue, gel-state electrolytes may represent a good solution in order to maintain stability and good performances, albeit at lower costs. In the present work, two different kinds of gel-electrolytes, based on poly (methyl methacrylate) (PMMA) and nanoclay agents, were investigated in DSSC-devices sensitized using β-substituted Zn-porphyrins (namely ZnPC4 and ZnPC12) with enveloping alkoxy chains of different lengths, able to produce a coverage of the photoanode surface. The highest power conversion efficiency (PCE) values equal to 1.06 ± 0.04% and 1.55 ± 0.26% were obtained for ZnPC12 (with longer alkoxy chains) with PMMA- and nanoclay-based electrolytes respectively. The properties of the photoanode/electrolyte interface as well as the influence of the gelling agents on the final properties of the obtained devices were thoroughly characterized.

Keywords: Dye-Sensitized Solar Cells; gel-state electrolytes; poly (methyl methacrylate); nanoclay; β-substituted Zn-porphyrins

Citation: Sangiorgi, N.; Sangiorgi, A.; Sanson, A.; Licchelli, M.; Orbelli Biroli, A. An Investigation on Gel-State Electrolytes for Solar Cells Sensitized with β-Substituted Porphyrinic Dyes. *Processes* **2023**, *11*, 463. https://doi.org/10.3390/pr11020463

Academic Editor: Christos Argirusis

Received: 27 December 2022
Revised: 18 January 2023
Accepted: 28 January 2023
Published: 3 February 2023

1. Introduction

The current depletion of fossil fuels to satisfy a continuous growth of energy demand has given rise to dramatic environmental and climate changes due to an increment in greenhouse gas emissions. To limit these issues, the search and the development of new and more efficient devices for the exploitation of alternative renewable sources have been pursued. In the photovoltaic field, Dye-Sensitized Solar Cells (DSSCs) have been extensively investigated in recent years due to (i) the low cost of their raw materials [1] and fabrication processes; (ii) their transparency and colouring, making them ideal candidates to be integrated in the buildings envelop [2]; (iii) the better and even astonishing power conversion efficiencies (PCEs) of light into electricity in ambient diffuse-light condition [3]. The latter feature can be exploited in the indoor energy production industry, as well as in wearable and portable devices [4]. However, some challenges related to device performance and stability must be overcome, mainly improving the properties of the single device components [4–7]. Among them, considering a highly efficient DSSC architecture, the electrolyte is the only component in a liquid state, and it is deeply affected by leakage and evaporation phenomena. In order to exceed these issues, the liquid electrolyte should be replaced with a gel-state or solid-state one [8,9]. For these purposes, different kinds of materials can be used, including polymers, organic and inorganic nanoparticles, and Hole Transport Materials (HTM) for complete solid-state DSSCs [10–12]. Among the latter, the main limitation arises from the high costs and very low stability. The advantages of the gel-state electrolyte are related to their scalable and low-cost production process and the possibility to maintain the redox couple used in the liquid electrolyte [8]. For this purpose, bio-based polymer membranes, containing κ-carrageenan (κC) (a linear

sulfated polysaccharide extracted from seaweeds) prepared using chemical extraction and dissolved in 1 vol.% of acetic acid solutions, are used [13]. The transparent membranes are obtained after drying this solution at room temperature for 72 h. Synthetic polymers, such as poly(acrylonitrile) (PAN) mixed with ethylene carbonate (EC) and propylene carbonate (PC) in different weight ratio are also considered [14]. In this case, the gel-state electrolyte is achieved using gelatinization promoted by heating the solution at 100 °C. Another example is poly (ethylene oxide) (PEO) with PC and acetonitrile, in a v/v ratio of 1:20, and different amounts of urea to study its influence on ions mobility [15]. Gel-state electrolytes are then prepared using acetonitrile evaporation at 80 °C. Moreover, poly (methyl methacrylate) (PMMA) blended with PANI/NT, changing the weight percentages of PANI-NT in the PMMA polymer matrix, which is an alternative way to prepare gelled electrolytes [16]. The mixture of these components is maintained at 35 °C for 6 h to create the final polymer network. Finally, with the aim of producing quasi-solid-state electrolytes (QSSLs), copolymers such as poly (vinylidene fluoride-co-hexafluoropropylene) (PVDF-HFP) as a gelling agent in combination with 3-metoxypropionitrile are employed [17]. In this case, the polymeric compound is added to the liquid electrolyte and heated until complete solidification. Recently, PMMA was used to prepare a stable polymeric membrane consisting in polyindole and poly(3-decyl-1-vinyl imidazolium iodide) to produce stable gel-state DSSCs with a PCE of 5.96% [18]. These membranes were obtained by drying the electrolyte solution of precursors at 80 °C in a petri dich. Moreover, a nanocomposite polymer blend, based on (PVDF-HFP)/PMMA and TiO_2 nanofibers as a filler, was prepared and used as gel-state electrolyte that provided, in the best conditions (6 wt.% of TiO_2), devices with a PCE of 8.08% [19]. This blend was achieved using an electrospinning method, and the obtained fibers were calcined at 600 °C for 3 h to create crystalline anatase nanofibers. Moreover, DSSCs for indoor applications were fabricated using a cobalt complexed redox couple and gel-state electrolytes with an optimized amount of PVDF-HFP and PMMA polymers, providing PCE exceeding 25% under artificial light [20]. The quasi-solid electrolytes are achieved by gelling the liquid ones with different ratios of polymeric components.

Considering inorganic or organic nanoparticles as gelling materials (e.g., TiO_2, SiO_2, Al_2O_3, carbon-based materials), the highest performances were obtained for nanoclay-based systems due to their higher chemical stability, ion exchange capacity, and adequate rheological properties [8]. Mg-Al nanoclay materials are prepared using chemical synthesis (co-precipitation method) from magnesium and aluminium nitrate precursors [21,22]. A basic solution is then used to prepare the hydrolysed precipitate, which is maintained at pH 12 and 80 °C for 48 h. Finally, the nanoclay powder is washed with water and freeze dried for 8 h. The formulation protocol to obtain this type of electrolytes was simply based on gelling the liquid electrolyte by adding different amounts of nanoclay powders and mixing them using sonication. Finally, montmorillonite nanoclay was employed to create a composite gel-state electrolyte in combination with PVDF-HFP and an iodide/iodine redox couple that produced a DSSC with a PCE of 6.77% in the optimized conditions (5 wt.% of nanoclay) [23]. A critical aspect that must be considered with a gel-state electrolyte is related to its interaction with the photoanode side (TiO_2 active layer and sensitizer) and the corresponding properties of the TiO_2/dye/electrolyte interface. In this context, the chemical structure and electronic properties of the sensitizer are crucial. The results obtained for a gel-state electrolyte in combination with traditional ruthenium-based dyes and organic ones are reported in the literature. On the contrary, the combination of gel-state DSSCs with porphyrins as sensitizers is still practically unexplored, even if highly engineered push–pull *meso*-substituted Zn-porphyrins have shown PCEs over 13%, outperforming the ruthenium dyes [24–26]. There are just a few papers reporting the properties of DSSCs with porphyrins and solid-state electrolyte or ionic liquids [27–29].

In this work, we investigated the properties of DSSCs' coupling gel-state electrolytes based on PMMA or nanoclay, with β-substituted Zn-tetraarylporphyrins, which present a more straightforward synthesis than the *meso*-substituted [30] and, at the same time, have

shown good PCE performances of up to over 8% [31]. In particular, since the presence of a protective shield effect on the photoanode is also demanded in the case of gel electrolytes, we focused our attention on the **ZnPC12** molecule (see Figure 1) as a dye-sensitizer, bearing a dodecyloxy chain in the *ortho*-position of its phenyl moieties. The mono *ortho*-substitution was found to be more effective than the *ortho–ortho* (as in the case of *meso* push–pull porphyrins) and the *ortho–meta* substitution, both in terms of better PCEs and an easier synthesis [32]. Therefore, as a benchmark, it was compared with the **ZnPC4** with a shorter butoxyl chain (see Figure 1).

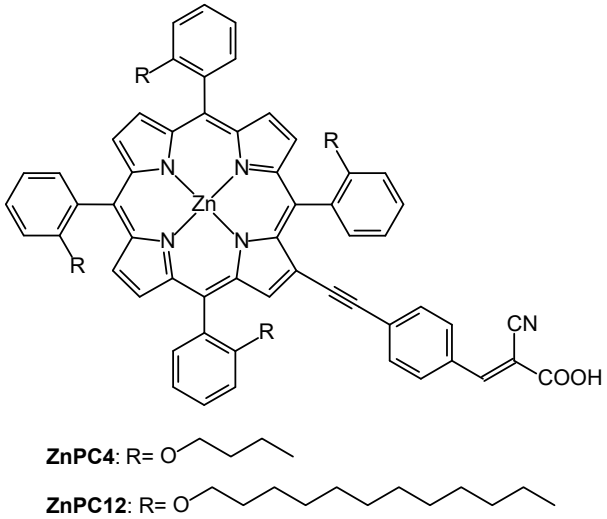

Figure 1. Dye-sensitizers investigated.

In principle, these two porphyrins have the same electronic features, and any difference in the device performances should be directly addressed to the different alkoxy chains length. When they were investigated in a DSSC with a liquid electrolyte, it was found that the longer chains produced a better PCE value due in particular to a high value of V_{OC}, which confirms the effectiveness against the recombination processes at the TiO_2/dye interface and thus the protective effect on the photoanode. Moreover, the presence of longer chains enables the limitation of dye-to-dye aggregation (porphyrins have a strong tendency to form π–π stacking aggregate) and the interaction between the zinc cation coordinated inside of the porphyrinic core with the I_3^- component of the electrolyte, promoting a faster recombination reaction with the injected electron [33].

Herein, the influence of the different gelling agents in combination with these porphyrins on both photovoltaic and electrochemical DSSC properties was determined and the influence on the devices' efficiencies was clarified.

2. Materials and Methods

2.1. Electrolyte Preparation

A previously optimized procedure to prepare the gel-state electrolyte based on poly methyl methacrylate (PMMA) was used [34]. In brief, aiming to facilitate the PMMA (average MW 120,000 g mol^{-1}, Sigma Aldrich, St. Louis, MO, USA) gelation, acetone (99.5%, Sigma–Aldrich, USA) was chosen as the aprotic polar solvent mainly for its high dissolving power and mild toxicity. The selected solvent (10 mL) was initially mixed with 0.35 g of polyethylene glycol (PEG 200, Merck, Darmstadt, Germany) to increase the gel plasticity; then, a proper amount of PMMA, equal to 0.25 g, was added, and the so-obtained solution was finally stirred at room temperature until a homogeneously clear product was produced. To conclude the electrolyte formulation and to boost the ionic conductivity, 0.4 g of ethylene carbonate (EC, 98% Sigma Aldrich, USA) was added to the system. The gel composition, after drying, was: PMMA 25 wt.%, PEG 35 wt.% and EC 40 wt.%. The final gelled electrolyte was obtained by directly mixing a commercial electrolyte solution based

on $3I^-/I_3^-$ (EL-HSE, Dyesol, West Perth, WA, Australia) with the gel mixture reaching an 80:20 wt.% ratio, respectively. Due to its reduced viscosity, the as-obtained solution was injected into the devices, employing a vacuum fill syringe; then, these prototypes were left to rest at room temperature for 20 min, allowing the complete acetone evaporation and thus obtaining the quasi-solid electrolyte. The gel-state electrolyte based on nanoclay was prepared by dispersing 5 wt.% of montmorillonite (size < 20 μm, Sigma–Aldrich, USA) into the previous commercial liquid electrolyte followed by a short sonication at room temperature. The as-prepared nanocaly gel electrolyte was then applied into the devices using a vacuum fill syringe. All the chemicals and materials used were stored in the dark and, where necessary, at −5 °C. The commercial products were stable at room temperature and pressure, and the only molecules synthesized were porphyrin dye, which are very stable molecules at the solid state and can be safely stored at room temperature too.

2.2. DSSCs Assembly

Firstly, to obtain the DSSC photoanode, a $TiCl_4$ solution (50×10^{-3} M in absolute ethanol) was spin-coated onto an FTO glass substrate that was subsequently thermally treated at 450 °C for 30 min [35] in order to produce a dense titanium dioxide-based blocking layer (BL). A commercial TiO_2 ink (Dyesol 18 NR-T, Dyesol, Australia) was then applied onto the BL by screen-printing (AUR'EL 900, AUR'EL Automation s.p.a., Modigliana, Italy) and sintered at the same BL conditions. The final TiO_2 film thickness was set at 8 μm as confirmed by using a profilometer (Optical 3D Microscope, Bruker, Billerica, MA, USA). After sintering, and aiming to increase the film-specific surface area, the samples were dipped into a hot 5×10^{-3} M $TiCl_4$ aqueous solution and then fired at 450 °C for 30 min. The as-obtained photoanodes were sensitized for 4 h with the ZnPC12 and ZnPC4 solutions (2×10^{-4} M) in tetrahydrofuran (≥99.9%, Sigma Aldrich): absolute ethanol 1:9 vol.%. The sensitization step was carried out in the presence of chenodeoxycholic acid (2×10^{-3} M, Solaronix, Aubonne, Switzerland), which was used as a disaggregating agent. Pre-drilled FTO glasses were coated using the sputtering method with Pt, producing suitable counter electrodes. Finally, sandwich-type cells were assembled by joining and sealing the electrodes with a hot melt gasket (Meltonix, thickness 25 μm, Solaronix) and then by introducing the gel-state electrolytes through the holes at the counter electrodes. The same polymer gasket was combined with small cover glasses to seal the holes. The solar cells' active area was fixed at 0.25 cm^2. All the reported devices were prepared at room temperature and in air conditions.

2.3. Characterizations and Measurements

Electronic absorption spectra of porphyrin dyes were acquired at room temperature in THF solution with a Shimadzu UV3600 spectrophotometer. Steady state emission spectra were measured in degassed THF solution with a FLS 980 spectrofluorimeter (Edinburgh Instrument Ltd., Livingston, UK) equipped with a 450 W Xenon arc lamp.

In order to determine the ionic conductivity of the gel-state electrolytes based on PMMA and nanoclay, Electrochemical Impedance Spectroscopy (EIS) analyses on symmetrical dummy cells (counter-electrode/electrolyte/counter-electrode) were performed. Two identical FTO glass substrates (sheet resistance 7 Ω/sq, Sigma Aldrich), which were covered with 3 nm Platinum thin films prepared using sputtering method and annealed at 500 °C for 30 min, were used. The dummy cells' active area was set at 0.25 cm^2. These two electrodes were sealed by using a 25 μm thick Meltonix sheet, and the space between them was filled with gel-state electrolyte using the holes previously created on the glass/FTO substrate. EIS was performed in the frequency range between 10^5 and 10^{-2} Hz with potential applied equal to 0 V and signal amplitude of 10 mV in dark conditions and room temperature. Concerning the DSSC characterizations, an Abet Technologies solar simulator (SUN 2000, Milford, CT, USA) equipped with a Keithley 2400 source meter was employed to record J–V curves under AM 1.5 and 1000 W m^{-2}. Moreover, the Incident Photon-to-Current Conversion Efficiency (IPCE) was determined to be in the wavelength

range between 300 and 800 nm, with an IPCE PVE300 system (Bentham, UK) operating with a dual Xenon/Quartz halogen light source. EIS analyses were carried out over a frequency range of 10^5 Hz to 10^{-2} Hz with an amplitude of 10 mV at the V_{OC} under the previously reported illumination conditions. The whole electrochemical characterizations were performed by using AUTOLAB PGSTAT302N-FRA32M (Eco Chemie, Utrecht, The Netherlands) combined with the Nova 2.1 software. EIS data fitting was realized employing the Z-View software (Scribner Associates, Southern Pines, NC, USA). Finally, DSSC prototypes were stressed by undergoing long-term stability tests (1000 h); moreover, the devices were stored in the dark prior to being tested for the first time at room conditions (25 °C and 1 atmosphere). For each DSSC, after every 200, 560, and 1000 h, the J–V curves under illumination (under AM 1.5 and 1000 W m^{-2}) were acquired.

3. Results and Discussion

3.1. Spectroscopic Features and Energy Levels of Dyes

ZnPC4 and **ZnPC12** was synthesized as previously reported in the literature [33]. In Figure 2, for reader support, we report the absorption and emission spectra recorded in the THF solution.

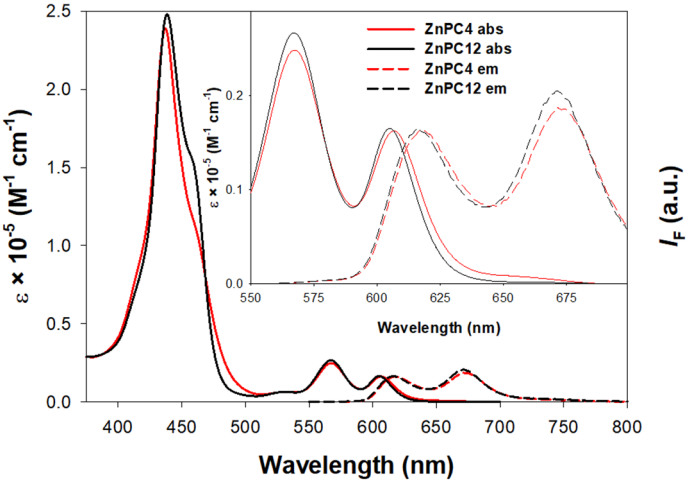

Figure 2. ε-normalized absorption spectra and normalized emission spectra (1 μM conc., $\lambda_{exc.}$ = 445 nm) of **ZnPC4** and **ZnPC12** in THF solution.

Both the absorption spectra show the typical pattern of a metalloporphyrin consisting in an intense absorption band at higher energy (436–438 nm) with a shoulder at around 460 nm, which can be justified by the presence of the strong electron-acceptor cyanoacrylic group [36]. At lower energy, two less intense bands (namely the Q-bands) are present with the relative peaks in the range between 567 and 606 nm ca. In the same figure, we also report the emission spectra, which reflect the Q-band's absorption pattern. In addition, it is possible to observe a small Stokes' shift between the absorption peak at lower energy and the emission peak at higher energy: this proves the rigidity of the systems and that any distortions of the molecular structures do not occur during the absorption and emission processes. The observed E^{0-0} values allow us to assess the spectroscopic highest occupied molecular orbital–lowest unoccupied molecular orbital (HOMO–LUMO) gap, which was found to be 1.98 and 1.99 eV for **ZPC4** and **ZPC12**, respectively. These values are lower than those already reported as 2.09 and 2.11 eV, respectively, and were obtained only from the electrochemical data [33].

The HOMO values were obtained from the E°' of the first anodic peak in cyclovoltammetry (−5.07 eV and −5.09 eV, at lower potentials with respect to I^-/I_3^- redox shuttle, −4.85 eV) [33] and allow us to calculate the spectroscopic LUMO energy levels: −3.09 eV and −3.10 eV for **ZPC4** and **ZPC12**, respectively. These latter values are lower compared to the electrochemical LUMO data (−2.98 and −2.97 eV) previously reported [33]. Never-

theless, they have a sufficient higher energy value compared to the TiO_2 conduction band value (−3.94 eV), ensuring the charge injection from their excited states.

3.2. Characterization of Gel-Electrolytes

The EIS spectra of the different gel-state electrolytes, tested in a symmetrical cell set-up, and the equivalent circuit built to fit the experimental points are reported in Figure 3. The Nyquist plots consist of two semicircles at high (on the left) and low frequency (on the right) corresponding to the electrode–electrolyte interface and ions' diffusion. Concerning the elements of the equivalent circuit, R1 describes the electrical resistance due to the substrate and the film adhesion, R2 and CPE1 represent the charge-transfer resistance and capacitance of the electrode/electrolyte interface, and Ws1 describe the Nernst diffusion impedance for the iodine-based gel state electrolyte [37].

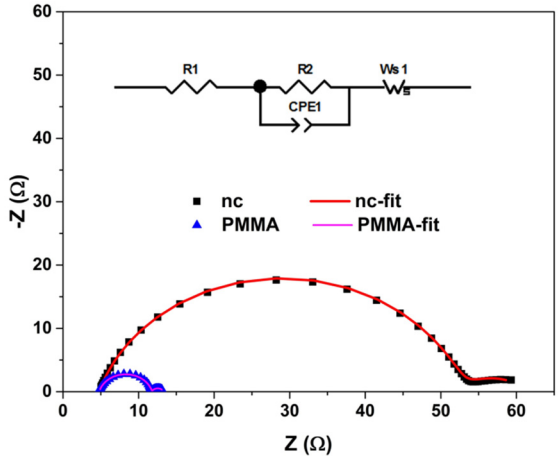

Figure 3. Nyquist plots of symmetrical cells with gel-state electrolytes based on PMMA or nanoclay with equivalent circuit used.

According to the electrolyte resistance (Rb), determined by fitting the spectra with the equivalent circuit in Figure 3, and equal to 11.6 Ω and 52.4 Ω for PMMA and nanoclay, respectively, the electrolytes' ionic conductivity (σ) was calculated using the following equation [38]:

$$\sigma = \frac{t}{R_b} \times \frac{1}{A}$$

where t is the thickness of the electrolyte film (2.5×10^{-3} cm) and A is the area of the electrode (2.5×10^{-1} cm^{-2}). The as-obtained ionic conductivity is equal to 1.9×10^{-4} S cm^{-1} and 8.5×10^{-4} S cm^{-1} for nanoclay and PMMA, respectively. Moreover, the diffusion coefficient D_n was calculated using the W_s-T element (values from EIS fitting equal to 1.06 s^{-1} and 2.59 s^{-1} were obtained for PMMA and nanoclay, respectively) related to the Warburg finite impedance and the equation below [34]:

$$D_n = \frac{t^2}{W_S - T}$$

The obtained values are equal to 5.8×10^{-6} cm^2 s^{-1} and 2.4×10^{-6} cm^2 s^{-1} for PMMA and nanoclay, respectively. The "diffusion interpretation" element (W_s-T), related to the Warburg finite impedance, was obtained from the equivalent circuit used to fit the experimental points of the Nyquist plot. Ws-T describes the overall Warburg impedance with other two components: the diffusion impedance (W_s-R) and an exponential factor (W_s-P) that indicates Warburg diffusion when equal to 0.5. The highest ionic conductivity and diffusion coefficient founded for the PMMA gel electrolyte was due to the three-dimensional polymeric framework that is able to maintain the high charge mobility of the liquid part of

the electrolyte trapped inside. Moreover, the polymeric electrolyte incorporates both the diffusive properties of fluids and the cohesive property of the solid [39]. A different ionic conduction mechanism was obtained when nanoclay was used as the gelling agent. Due to the electrostatic forces between the faces and edges of the clay platelets, a unique network forms in the fluid and turns the liquid to gel. When a network of a nanoclay is formed, the solvent can be related in the gel through physical and chemical interactions between the solvent and nanoclay [40]. This behaviour is explained by two parallel charge transport process: normal physical diffusion and Grotthus-type bond exchange. This is due to the interaction of a $3I^-/I_3^-$ redox couple with the nanoclay, in which a significant portion of the iodine ions are adsorbed on the surface of the clay. Moreover, lower charge-transfer resistance at the Platinum electrode was obtained for the PMMA electrolyte than the one based on nanoclay, the recorded values for which were 7 and 48 Ω for PMMA and nanoclay electrolytes, respectively. This result confirms the best catalytic and conduction properties of the PMMA-based electrolyte.

3.3. Photoelectrochemical Investigation

The best current density–voltage curves (J-V), both in the dark and under illumination, of the DSSCs sensitized with Zn-porphyrins **ZnPC4** and **ZnPC12** and filled with PMMA and nanoclay gel state electrolytes (1000 W m^{-2} AM 1.5) are reported in Figure 4A,B, respectively. The extrapolated photovoltaic parameters (considering 5 DSSC prototypes) are reported in Table 1.

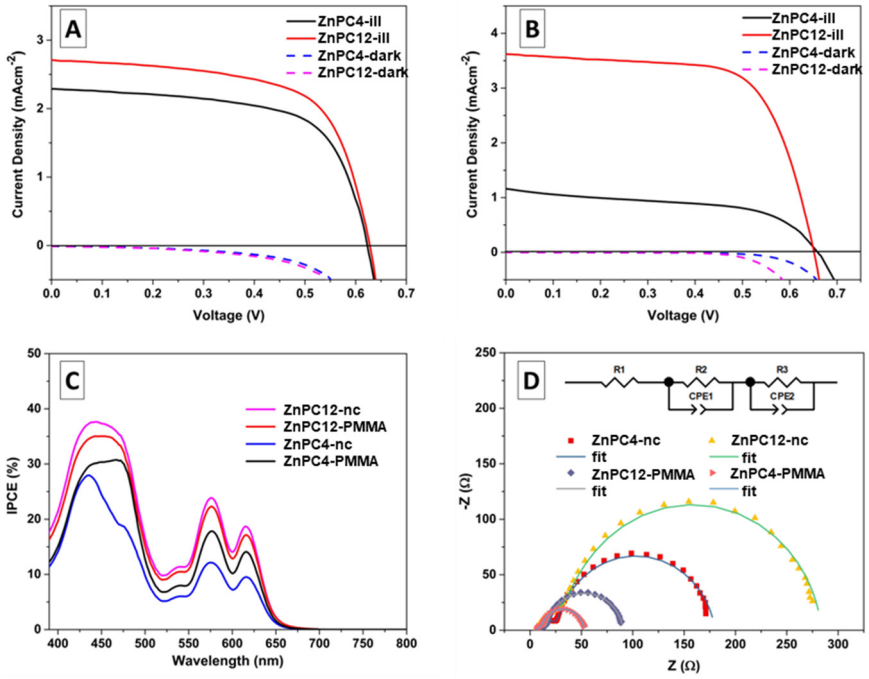

Figure 4. J–V curves under illumination and in the dark for DSSCs with PMMA electrolyte (**A**) and nanoclay (**B**). IPCE spectra of the related devices (**C**). Nyquist plots of the DSSCs under illumination with equivalent circuit used (**D**).

Table 1. Photovoltaic parameters for DSSCs based on PMMA and nanoclay electrolytes.

		J_{SC} (mA cm^{-2})	V_{OC} (mV)	FF (%)	PCE (%)
PMMA	ZnPC4	2.26 ± 0.03	616 ± 7	62 ± 3	0.87 ± 0.05
	ZnPC12	2.68 ± 0.14	620 ± 9	63 ± 1	1.06 ± 0.04
nanoclay	ZnPC4	1.19 ± 0.25	639 ± 15	52 ± 2	0.39 ± 0.06
	ZnPC12	3.59 ± 0.45	651 ± 11	67 ± 2	1.55 ± 0.26

The results summarized in Table 1 show slight differences between the PCEs of the devices with the PMMA electrolyte while the highest PCE differences were found for the different Zn-porphyrins with the nanoclay electrolyte. These results are due to the different interactions between dyes and gel-state electrolytes. The **ZnPC12** molecule was able to reach the highest PCE (1.55 ± 0.26% and 1.06 ± 0.04% for nanocaly and PMMA, respectively) and J_{SC} (3.59 ± 0.45 mA cm^{-2} and 2.68 ± 0.14 mA cm^{-2} for nanocaly and PMMA, respectively) values for both electrolytes. The same trend observed from J_{SC} was obtained also in the IPCE analyses (Figure 4C), wherein the DSSCs based on the **ZnPC12** dye reached the highest IPCE values. These results are directly comparable and confirmed by the adsorption spectra acquired on the photoanodes sensitized with the different dyes (Figure 5).

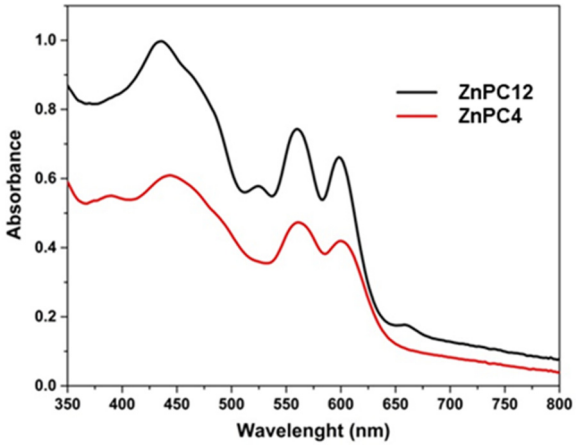

Figure 5. Adsorption spectra of sensitized photoanodes with **ZnPC12** and **ZnPC4**.

Considering the same amount of dyes adsorbed on the TiO_2 particle surfaces, the **ZnPC12** dye shows better light harvesting capability than the **ZnPC4** due to its reduced self-aggregation, as ensured by the length of the dodecyloxy chain [33]. The aggregates formation is detrimental for the absorption properties of these dyes when they are attached to the TiO_2 surface, thus limiting the efficiency of charge injection from the excited state of the dye to the semiconductor. Consequently, in the case of **ZnPC4**, we observed lower Jsc values. This parameter was dramatically lower in the case of the nanoclay's gel electrolyte. This evidence suggests that the PMMA has the same organic nature as the dye alkoxy chains and that it can therefore effectively interact at the interface, with the porphyrin film helping in the disaggregation of the molecules. On the other hand, the nanoclays, being inorganic materials, are not able to perform the same interactions, leading to aggregation phenomena that strongly affect the **ZnPC4** dye efficiency in light-harvesting and the relative charge injection processes.

The influence of the gel-state electrolyte was observed on the V_{OC} parameter, where the nanoclay produced the highest values (639 ± 15 mV and 651 ± 11 mV for **ZnPC4** and **ZnPC12**, respectively). The literature reports that the the addition of nitrate–hydrotalcite clay in the electrolyte has the effect of buffering the protonation process at the TiO_2/electrolyte interface, resulting in an upward shift in the conduction band and a boost in open circuit voltage [21,22,40]. Moreover, the highest V_{OC} values recorded for the nanoclay-based electrolyte is probably due to the low recombination rate between the TiO_2/dye and electrolyte. In fact, the dark current's onset (Figure 4A,B) takes place at low bias for PMMA-based electrolytes while the nanoclay-based DSSCs repress the dark currents, thus shifting their onset at higher potentials [41]. In order to deeply explain these results, EIS analyses were repeated under illumination, and the relative Nyquist plots and equivalent circuit used to fit the experimental points are depicted in Figure 4D. The presence of two main semicircles at high and medium frequencies, attributable to charge transfer processes occurring at the counter-electrode and TiO_2 photoanode side, respectively [42], are clearly

visible in the Nyquist plots. We assuming that, in the reported equivalent circuit, R1 is the sum of the series' resistances caused by the electrode materials and the electrical connections, R2/CPE1 (constant phase element) represents the counter-electrode/electrolyte interface electronic properties, and, finally, that R3/CPE2 describes the electronic properties of dye/TiO_2/electrolyte interfaces [43]. R3 values for **ZnPC4**-PMMA, **ZnPC12**-PMMA, **ZnPC4**-nanoclay, and **ZnPC12**-nanoclay were found equal to 42, 75, 154, 248 Ω, respectively. These results agree with the trend of V_{OC} values reported in Table 1. An increase in the R3 values means a reduced recombination of the photogenerated carriers that finally increase the V_{OC}.

Finally, long-term stability tests were conducted, and the obtained results are reported in Figure 6.

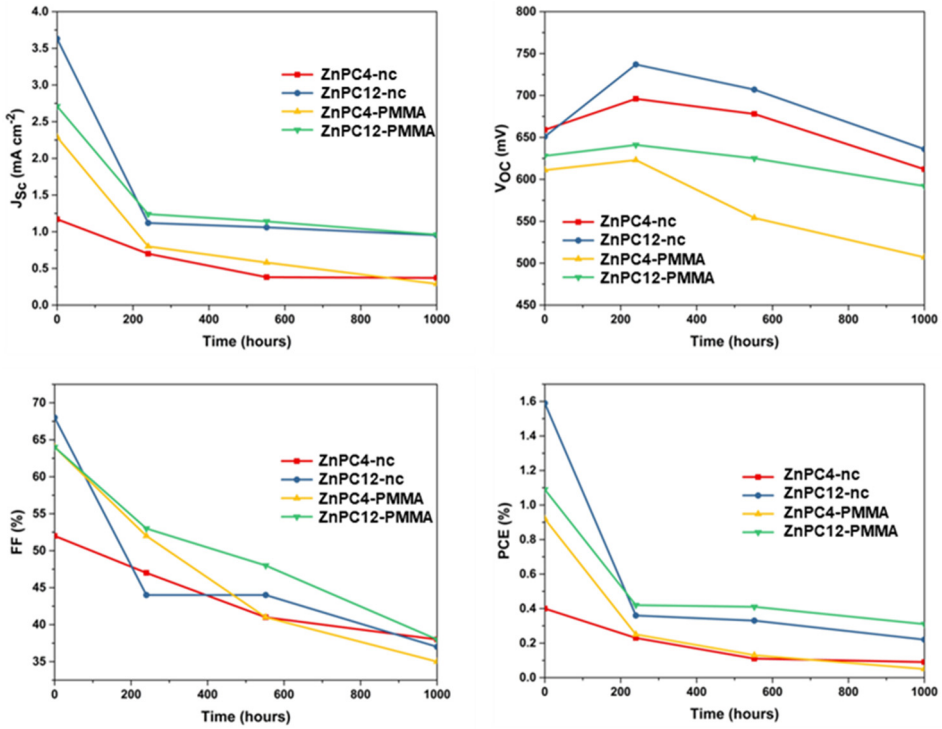

Figure 6. Photovoltaic parameters extrapolated during long-term stability tests.

Figure 6 shows a comparable stability between the two different gel-state electrolytes. For the nanoclay electrolyte, as expected, the V_{OC} initially increases due to the equilibrium process that occurs between inorganic nanoparticles and the liquid electrolyte [39].

4. Conclusions

In this paper, we have reported the coupling of two β-substituted Zn-porphyrins bearing peripheral alkoxy chains of different lengths (namely **ZnPC4** and **ZnPC12**), with the gel electrolyte being based on PMMA and nanoclay in DSSC devices.

ZnPC4 and **ZnPC12** have roughly the same electronic and spectroscopic properties, but the longer dodecyloxy chains prevent the formation of aggregates at the TiO_2 mesoporous film surface, resulting in higher light absorption on the photoanode and, consequently, in higher PCE values for **ZnPC12**, both with a PMMA- and nanoclay-based electrolyte. In particular, **ZnPC12** combined with the nanoclay electrolyte shows an increment in the PCE values of about 46% compared to the device with the PMMA electrolyte. On the contrary, **ZnPC4** presents a higher PCE value when it is coupled with the PMMA electrolyte: this fact may be attribute to a beneficial effect of PMMA on the aggregated dyes. This latter aspect is confirmed by the IPCE spectra, where the photon-to-current conversion is higher for **ZnPC4** with the PMMA electrolyte, while only a slightly better

efficiency is observed in the case of **ZnPC12** with the nanocaly electrolyte. EIS spectroscopy measurements fully corroborate the above considerations.

Moreover, stability experiments indicate that, after an initial decrement (until 200 h ca.), the efficiency values decrease very slowly, reflecting the same trend of the J_{SC} values.

Both PMMA and nanoclay electrolytes are suitable to build gel-state DSSCs with a Zn-porphyrin dye; however, the stability of these devices should be increased to optimize the electrolyte formulation (changing the amount of nanoclay or polymer, additives, and plasticizers) and to improve the properties of the cell sealant.

Finally, both PMMA and nanoclay electrolytes are suitable to build a gel-state DSSC with Zn-porphyrins. The development of this kind of gel-state electrolyte can improve the flexibility and efficiency of this DSSC component. In fact, employing gelling agents as PMMA or nanoclay instead of p-type materials as hole transport materials allows one to introduce the liquid electrolyte booster molecules to enhance the PCE and ionic conductivities, as well as some stabilizers. With this innovative approach, stable and more efficient gel-state electrolytes should be developed.

Author Contributions: Conceptualization, N.S. and A.O.B.; methodology, N.S.; validation, N.S., A.S. (Alex Sangiorgi) and A.O.B.; formal analysis, N.S. and A.S. (Alex Sangiorgi); investigation, N.S., A.S. (Alex Sangiorgi) and A.O.B.; resources, A.S. (Alessandra Sanson), M.L. and A.O.B.; writing—original draft preparation, N.S. and A.S. (Alex Sangiorgi); writing—review and editing, N.S., A.S. (Alex Sangiorgi), M.L. and A.O.B.; visualization, N.S., A.S. (Alex Sangiorgi), M.L. and A.O.B.; supervision, N.S. and A.O.B.; project administration, N.S. and A.S. (Alessandra Sanson); funding acquisition, A.S. (Alessandra Sanson) and M.L. All authors have read and agreed to the published version of the manuscript.

Funding: This research received no external funding.

Institutional Review Board Statement: Not applicable.

Informed Consent Statement: Not applicable.

Data Availability Statement: The data presented in this research study are available in the present article.

Conflicts of Interest: The authors declare no conflict of interest.

References

1. Sangiorgi, N.; Sangiorgi, A.; Sanson, A. Seawater-Based Electrolytes Facilitate Charge Transfer Mechanisms Improving the Efficiency of Dye-Sensitized Solar Cells. *J. Electroanal. Chem.* **2022**, *915*, 116352. [CrossRef]
2. Muñoz-García, A.B.; Benesperi, I.; Boschloo, G.; Concepcion, J.J.; Delcamp, J.H.; Gibson, E.A.; Meyer, G.J.; Pavone, M.; Pettersson, H.; Hagfeldt, A.; et al. Dye-Sensitized Solar Cells Strike Back. *Chem. Soc. Rev.* **2021**, *50*, 12450–12550. [PubMed]
3. Haridas, R.; Velore, J.; Pradhan, S.C.; Vindhyasarumi, A.; Yoosaf, K.; Soman, S.; Unni, K.N.N.; Ajayaghosh, A. Indoor Light-Harvesting Dye-Sensitized Solar Cells Surpassing 30% Efficiency without Co-Sensitizers. *Mater. Adv.* **2021**, *2*, 7773–7787. [CrossRef]
4. Michaels, H.; Benesperi, I.; Freitag, M. Challenges and Prospects of Ambient Hybrid Solar Cell Applications. *Chem. Sci.* **2021**, *12*, 5002–5015. [CrossRef]
5. Wu, C.; Wang, K.; Batmunkh, M.; Bati, A.S.R.; Yang, D.; Jiang, Y.; Hou, Y.; Shapter, J.G.; Priya, S. Multifunctional Nanostructured Materials for next Generation Photovoltaics. *Nano Energy* **2020**, *70*, 104480. [CrossRef]
6. Rondán-Gómez, V.; Montoya De Los Santos, I.; Seuret-Jiménez, D.; Ayala-Mató, F.; Zamudio-Lara, A.; Robles-Bonilla, T.; Courel, M. Recent Advances in Dye-Sensitized Solar Cells. *Appl. Phys. A* **2019**, *125*, 1–24. [CrossRef]
7. Fasolini, A.; Sangiorgi, N.; Tosi Brandi, E.; Sangiorgi, A.; Mariani, F.; Scavetta, E.; Sanson, A.; Basile, F. Increased Efficiency and Stability of Dye-Sensitized Solar Cells (DSSC) Photoanode by Intercalation of Eosin Y into Zn/Al Layered Double Hydroxide. *Appl. Clay Sci.* **2021**, *212*, 106219. [CrossRef]
8. Iftikhar, H.; Sonai, G.G.; Hashmi, S.G.; Nogueira, A.F.; Lund, P.D. Progress on Electrolytes Development in Dye-Sensitized Solar Cells. *Materials* **2019**, *12*, 1998. [CrossRef] [PubMed]
9. Mohamad, A.A. Physical Properties of Quasi-Solid-State Polymer Electrolytes for Dye-Sensitised Solar Cells: A Characterisation Review. *Sol. Energy* **2019**, *190*, 434–452. [CrossRef]
10. Benesperi, I.; Michaels, H.; Freitag, M. The Researcher's Guide to Solid-State Dye-Sensitized Solar Cells. *J. Mater. Chem. C* **2018**, *6*, 11903–11942. [CrossRef]
11. Saygili, Y.; Stojanovic, M.; Kim, H.S.; Teuscher, J.; Scopelliti, R.; Freitag, M.; Zakeeruddin, S.M.; Moser, J.E.; Grätzel, M.; Hagfeldt, A. Liquid State and Zombie Dye Sensitized Solar Cells with Copper Bipyridine Complexes Functionalized with Alkoxy Groups. *J. Phys. Chem. C* **2020**, *124*, 7071–7081. [CrossRef]

12. Sutton, M.; Lei, B.; Michaels, H.; Freitag, M.; Robertson, N. Rapid and Facile Fabrication of Polyiodide Solid-State Dye-Sensitized Solar Cells Using Ambient Air Drying. *ACS Appl. Mater. Interfaces* **2022**, *14*, 43456–43462. [CrossRef] [PubMed]
13. Bella, F.; Mobarak, N.N.; Jumaah, F.N.; Ahmad, A. From Seaweeds to Biopolymeric Electrolytes for Third Generation Solar Cells: An Intriguing Approach. *Electrochim. Acta* **2015**, *151*, 306–311. [CrossRef]
14. Sakali, S.M.; Khanmirzaei, M.H.; Lu, S.C.; Ramesh, S.; Ramesh, K. Investigation on Gel Polymer Electrolyte-Based Dye-Sensitized Solar Cells Using Carbon Nanotube. *Ionics* **2019**, *25*, 319–325. [CrossRef]
15. Pavithra, N.; Velayutham, D.; Sorrentino, A.; Anandan, S. Poly(Ethylene Oxide) Polymer Matrix Coupled with Urea as Gel Electrolyte for Dye Sensitized Solar Cell Applications. *Synth. Met.* **2017**, *226*, 62–70. [CrossRef]
16. Mohan, K.; Bora, A.; Nath, B.C.; Gogoi, P.; Saikia, B.J.; Dolui, S.K. A Highly Stable and Efficient Quasi Solid State Dye Sensitized Solar Cell Based on Polymethyl Methacrylate(PMMA)/Polyaniline Nanotube(PANI-NT) Gel Electrolyte. *Electrochim. Acta* **2016**, *222*, 1072–1078. [CrossRef]
17. Hwang, D.K.; Nam, J.E.; Jo, H.J.; Sung, S.J. Quasi-Solid State Electrolyte for Semi-Transparent Bifacial Dye-Sensitized Solar Cell with over 10% Power Conversion Efficiency. *J. Power Source* **2017**, *361*, 87–95. [CrossRef]
18. Thomas, M.; Rajiv, S. Porous Membrane of Polyindole and Polymeric Ionic Liquid Incorporated PMMA for Efficient Quasi-Solid State Dye Sensitized Solar Cell. *J. Photochem. Photobiol. A Chem.* **2020**, *394*, 112464. [CrossRef]
19. Subramanian, V.; Hari Prasad, K.; Das, H.T.; Ganapathy, K.; Nallani, S.; Maiyalagan, T. Novel Dispersion of 1D Nanofiber Fillers for Fast Ion-Conducting Nanocomposite Polymer Blend Quasi-Solid Electrolytes for Dye-Sensitized Solar Cells. *ACS Omega* **2022**, *7*, 1658–1670. [CrossRef]
20. Liu, I.P.; Cho, Y.S.; Teng, H.; Lee, Y.L. Quasi-Solid-State Dye-Sensitized Indoor Photovoltaics with Efficiencies Exceeding 25%. *J. Mater. Chem. A* **2020**, *8*, 22423–22433. [CrossRef]
21. Wang, X.; Kulkarni, S.A.; Ito, B.I.; Batabyal, S.K.; Nonomura, K.; Wong, C.C.; Grätzel, M.; Mhaisalkar, S.G.; Uchida, S. Nanoclay Gelation Approach toward Improved Dye-Sensitized Solar Cell Efficiencies: An Investigation of Charge Transport and Shift in the TiO_2 Conduction Band. *ACS Appl. Mater. Interfaces* **2013**, *5*, 444–450. [CrossRef] [PubMed]
22. González Pedro, V.; Sakurai, H.; Tomita, M.; Ito, B.I.; Fabregat Santiago, F.; Uchida, S.; Segawa, H. Impedance Spectroscopic Analysis of High-Performance Dye Sensitized Solar Cells Based on Nano-Clay Electrolytes. *Electrochim. Acta* **2016**, *197*, 77–83. [CrossRef]
23. Chen, L.H.; Venkatesan, S.; Liu, I.P.; Lee, Y.L. Highly Efficient Dye-Sensitized Solar Cells Based on Poly(Vinylidene Fluoride-Co-Hexafluoropropylene) and Montmorillonite Nanofiller-Based Composite Electrolytes. *J. Oleo Sci.* **2020**, *69*, 539–547. [CrossRef]
24. Higashino, T.; Imahori, H. Porphyrins as Excellent Dyes for Dye-Sensitized Solar Cells: Recent Developments and Insights. *Dalton Trans.* **2015**, *44*, 448–463. [CrossRef] [PubMed]
25. Mathew, S.; Yella, A.; Gao, P.; Humphry-Baker, R.; Curchod, B.F.E.; Ashari-Astani, N.; Tavernelli, I.; Rothlisberger, U.; Nazeeruddin, M.K.; Grätzel, M. Dye-Sensitized Solar Cells with 13% Efficiency Achieved through the Molecular Engineering of Porphyrin Sensitizers. *Nat. Chem.* **2014**, *6*, 242–247. [CrossRef] [PubMed]
26. Urbani, M.; Gra, M.; Nazeeruddin, M.K.; Grätzel, M.; Nazeeruddin, M.K.; Torres, T. Meso-Substituted Porphyrins for Dye-Sensitized Solar Cells. *Chem. Rev.* **2014**, *114*, 12330–12396. [CrossRef]
27. Armel, V.; Pringle, J.M.; Wagner, P.; Forsyth, M.; Officer, D.; MacFarlane, D.R. Porphyrin Dye-Sensitised Solar Cells Utilising a Solid-State Electrolyte. *Chem. Commun.* **2011**, *47*, 9327–9329. [CrossRef] [PubMed]
28. Armel, V.; Pringle, J.M.; Forsyth, M.; MacFarlane, D.R.; Officer, D.L.; Wagner, P. Ionic Liquid Electrolyte Porphyrin Dye Sensitised Solar Cells. *Chem. Commun.* **2010**, *46*, 3146–3148. [CrossRef] [PubMed]
29. Campbell, W.M.; Jolley, K.W.; Wagner, P.; Wagner, K.; Walsh, P.J.; Gordon, K.C.; Schmidt-Mende, L.; Nazeeruddin, M.K.; Wang, Q.; Grätzel, M.; et al. Highly Efficient Porphyrin Sensitizers for Dye-Sensitized Solar Cells. *J. Phys. Chem. C* **2007**, *111*, 11760–11762. [CrossRef]
30. Di Carlo, G.; Orbelli Biroli, A.; Pizzotti, M.; Tessore, F. Efficient Sunlight Harvesting by A4 β-Pyrrolic Substituted Zn^{II} Porphyrins: A Mini-Review. *Front. Chem.* **2019**, *7*, 177. [CrossRef]
31. Covezzi, A.; Orbelli Biroli, A.; Tessore, F.; Forni, A.; Marinotto, D.; Biagini, P.; Di Carlo, G.; Pizzotti, M. 4D–π–1A Type β-Substituted Zn^{II}-Porphyrins: Ideal Green Sensitizers for Building-Integrated Photovoltaics. *Chem. Commun.* **2016**, *52*, 12642–12645. [CrossRef]
32. Orbelli Biroli, A.; Tessore, F.; Vece, V.; Di Carlo, G.; Mussini, P.R.; Trifiletti, V.; de Marco, L.; Giannuzzi, R.; Manca, M.; Pizzotti, M. Highly Improved Performance of Zn^{II} Tetraarylporphyrinates in DSSCs by the Presence of Octyloxy Chains in the Aryl Rings. *J. Mater. Chem. A* **2015**, *3*, 2954–2959. [CrossRef]
33. Magnano, G.; Marinotto, D.; Cipolla, M.P.; Trifiletti, V.; Listorti, A.; Mussini, P.R.; Di Carlo, G.; Tessore, F.; Manca, M.; Orbelli Biroli, A.; et al. Influence of Alkoxy Chain Envelopes on the Interfacial Photoinduced Processes in Tetraarylporphyrin-Sensitized Solar Cells. *Phys. Chem. Chem. Phys.* **2016**, *18*, 9577–9585. [CrossRef] [PubMed]
34. Bendoni, R.; Barthélémy, A.L.; Sangiorgi, N.; Sangiorgi, A.; Sanson, A. Dye-Sensitized Solar Cells Based on N719 and Cobalt Gel Electrolyte Obtained through a Room Temperature Process. *J. Photochem. Photobiol. A Chem.* **2016**, *330*, 8–14. [CrossRef]
35. Sangiorgi, A.; Bendoni, R.; Sangiorgi, N.; Sanson, A.; Ballarin, B. Optimized TiO_2 Blocking Layer for Dye-Sensitized Solar Cells. *Ceram. Int.* **2014**, *40*, 10727–10735. [CrossRef]
36. Earles, J.C.; Gordon, K.C.; Stephenson, A.W.I.; Partridge, A.C.; Officer, D.L. Spectroscopic and Computational Study of β-Ethynylphenylene Substituted Zinc and Free-Base Porphyrins. *Phys. Chem. Chem. Phys.* **2011**, *13*, 1597–1605. [CrossRef]

37. Bella, F.; Porcarelli, L.; Mantione, D.; Gerbaldi, C.; Barolo, C.; Grätzel, M.; Mecerreyes, D. A Water-Based and Metal-Free Dye Solar Cell Exceeding 7% Efficiency Using a Cationic Poly(3,4-Ethylenedioxythiophene) Derivative. *Chem. Sci.* **2020**, *11*, 1485–1493. [CrossRef]
38. Yee, L.P.; Farhana, N.K.; Omar, F.S.; Sundararajan, V.; Bashir, S.; Saidi, N.M.; Ramesh, S.; Ramesh, K. Enhancing Efficiency of Dye Sensitized Solar Cells Based on Poly(Propylene) Carbonate Polymer Gel Electrolytes Incorporating Double Salts. *Ionics* **2020**, *26*, 493–502. [CrossRef]
39. Ngai, K.S.; Ramesh, S.; Ramesh, K.; Juan, J.C. A Review of Polymer Electrolytes: Fundamental, Approaches and Applications. *Ionics* **2016**, *22*, 1259–1279. [CrossRef]
40. Ding, B.; Jung, Y.; Kim, D.H.; Seong, W.M.; Kim, S.D.; Woo, S.K.; Lee, J.K. Rheological and Electrochemical Properties of Nanoclay Added Electrolyte for Dye Sensitized Solar Cells. *Electrochim. Acta* **2014**, *144*, 275–281. [CrossRef]
41. Bendoni, R.; Sangiorgi, N.; Sangiorgi, A.; Sanson, A. Role of Water in TiO_2 Screen-Printing Inks for Dye-Sensitized Solar Cells. *Sol. Energy* **2015**, *122*, 497–507. [CrossRef]
42. Liberatore, M.; Decker, F.; Burtone, L.; Zardetto, V.; Brown, T.M.; Reale, A.; di Carlo, A. Using EIS for Diagnosis of Dye-Sensitized Solar Cells Performance. *J. Appl. Electrochem.* **2009**, *39*, 2291–2295. [CrossRef]
43. Lin, R.Y.-Y.; Wu, F.L.; Chang, C.H.; Chou, H.H.; Chuang, T.M.; Chu, T.C.; Hsu, C.Y.; Chen, P.W.; Ho, K.C.; Lo, Y.H.; et al. Y-Shaped Metal-Free D-π-$(A)_2$ Sensitizers for High-Performance Dye-Sensitized Solar Cells. *J. Mater. Chem. A* **2014**, *2*, 3092–3101. [CrossRef]